Tailoring the Proton Conductivity and Microstructure of Block Copolymers by Countercation-Selective Membrane Fabrication

Huu-Dat Nguyen, Thi Khanh Ly Nguyen, Emilie Planes, Jacques Jestin, Lionel Porcar, Sandrine Lyonnard, Cristina Iojoiu

Tailoring the Proton Conductivity and Microstructure of Block Copolymers by Counter Cation-Selective Membrane Fabrication

*Huu-Dat Nguyen,[1,**] Thi Khanh Ly Nguyen,[1] Emilie Planes,[1] Jacques Jestin,[2] Lionel Procar,[3] Sandrine Lyonnard,[4,*] Cristina Iojoiu[1,*]*

[1]Univ. Grenoble Alpes, Univ. Savoie Mont Blanc, CNRS, Grenoble INP (Institute of Engineering Univ. Grenoble Alpes), LEPMI, UMR5279, 38000 Grenoble, France

[2]Laboratoire Léon Brillouin (LLB), CEA Saclay, CEA–CNRS–Université Paris Saclay, 91191 Gif-sur-Yvette Cedex, France

[3]Institut Laue Langevin (ILL), 38000 Grenoble, France

[4]Univ. Grenoble Alpes, CEA, CNRS, IRIG, SyMMES, F-38054 Grenoble, France

*Correspondence to:

C. Iojoiu (Cristina.Iojoiu@lepmi.grenoble-inp.fr)

S. Lyonnard (sandrine.lyonnard@cea.fr)

**Current address: Laboratoire Matériaux Batteries (LM)/STB/DEHT/LITEN, CEA Grenoble, 17 avenue des Martyrs, 38000 Grenoble, France

ABSTRACT

Here we report a simple-but-effective method to control the membrane morphology and transport properties of aromatic multi-block copolymers bearing perfluorosulfonic functions, via casting with different counter-cations. Five monovalent cations with different sizes, polarity, hydrophobicity, i.e., H^+, Li^+, K^+, Cs^+, TEA^+, and one double-valence cation, i.e., Ca^{2+}, were selected for manufacturing block copolymer membranes. We show that the counter-cation has a strong impact on the superstructure long-range order by acting as either block-separator, either block-compatibilizer, therefore tuning the thermodynamics of the self-assembly process. Hence, by selecting the cations, highly ordered or completely disordered phase-separated block morphologies can be created. The effect of counter-cation nature on the morphology is strongly reflected on the proton conductivity of acidified membranes. At 25 °C and 10% relative humidity, the acidified TEA^+-cast membranes are ~22 times less conductive than the acidified Cs^+-cast ones. By combining microscopy and neutron scattering techniques, we reveal the direct correlation between enhanced functional properties and quality of membrane microstructure directed by the nature of cations with beneficial characteristics. Our findings highlight the role and importance of cation selection to tailor the functional properties of multiblock ionomers applicable as solid electrolytes for energy conversion devices.

Keywords: Counter cation, membrane morphology control, Lewis acid strength, block copolymers, enhance membrane conductivity, perfluorosulfonic acid, SANS, polymer electrolyte

1. Introduction

Block copolymers are among the most studied class of polymers towards innovative applications due to their exceptional properties and modularity towards a broad range of applications. In the last decades, they were largely studied as polymer electrolytes for advanced electrochemical energy conversion and storage systems such as proton-exchange membrane fuel cells (PEMFCs),[1–3] anion-exchange membrane fuel cells (AEMFCs),[4,5] direct methanol fuel cells (DMFCs),[6,7] redox flow batteries (RFBs),[8] and lithium batteries (LIBs),[9,10] etc., owing to their ability to achieve essential and antagonist properties, *i.e.*, excellent thermomechanical strength and high ionic conductivity. In these materials, the nanostructured morphology derived from hydrophilic (ionic)-hydrophobic phase separation is the key to control the desired functional properties.[11–13] Indeed, the formation of an effective nanoscale ionic-channel network allowing interconnection of high mobility ionic pathways boosts ion transport across the membrane without affecting the mechanical strength.[14–16] The well-defined nanophase separation originates from the thermo-dynamical incompatibility between the two constitutive blocks.[17,18] Therefore, adequate molecular design and cast process could be combined to optimize self-assembly towards enhanced performances of the manufactured membrane for their application in real devices.

Cation-conducting aromatic block copolymers were largely investigated in view of energy applications due to their high thermal/electrochemical stability, low cost, ease of synthesis and modification towards desirable properties, etc.[10,19–22] The nanophase separation of ionic aromatic block copolymers, however, is hindered by (i) their highly rigid nature, (ii) the multi-block structure (iii) the relatively high polydispersity index (PDI) related to the synthesis process (*i.e.*, PDI close to 2 by polycondensation). To overcome these hurdles, much efforts were dedicated to design block structures with optimized block size,[11,23–25] or by introducing flexible perfluoroalkyl spacers.[26–29] In the latter case, the perfluoroalkyl spacer simultaneously improves (i) the formation of ionic clusters by increasing the phase separation between ionic side chains and rigid polymer main chains, and (ii) the acidity of acidic function by transforming aryl sulfonic acid (pKa=−1) into perfluorosulfonic acid (pKa=−6) with higher proton-dissociation ability.[30] Recently, post-synthesis strategies such as solvent selectivity[23,24] for film cast, thermal treatments,[24,31,32] crosslinking,[33–36] or applying electric field during film-cast process,[37–39] etc., have received much attention as possible ways to control membrane microstructure.

Here, we report an easy, simple and highly efficient method to tailor the block copolymer morphology and, consequently, to enhance the functional properties of proton conducting membranes based on aromatic ionomers, by selecting the counter-cations used during membrane manufacturing.

2. Results and Discussion

The influence of five monocharged cations M^+ with different radius, Lewis acid strength (LAS), hydrophobicity and organic/inorganic nature, namely H^+, Li^+, K^+, Cs^+, TEA^+ (**Figure 1a** and **Table S1**), on membrane morphology and proton transport properties was systematically studied. A double-charged cation, i.e., Ca^{2+}, is also considered. The ionomer is a multiblock copoly(arylene ether sulfone) bearing perfluorosulfonic acid functions (named "In", **Figure 1b-c**), synthesized as described elsewhere.[27] The molecular weight (MW) of both the FPES and PES blocks was fixed to 10000 g mol^{-1}. The MW of the ionic side chain was not taken into account, and the hydrophobic/hydrophilic block ratio is the same in all samples tested in this study. To obtain In polymers with different counter-cations, the acidic side chains were exchanged using 2M aqueous solution of corresponding metal-chloride (Li^+, Ca^{2+}, K^+, Cs^+) salts, or neutralized with triethylamine. The M^{z+}-form ionomers were cast from the non-selective solvent DMAc.[24] The resulting membranes (labeled In-M^{z+}, **Figure 1b**) were thermal annealed and then acidified to obtain proton conducting membranes (labeled In-M^{z+}/H^+, **Figure 1c**). For all samples, the ion-exchange capacities (IEC) measured by titration were found to be very close (1.27–1.30 meq. H^+/g, **Table S1**), indicating that most counter-cations were exchanged by protons in the acidified membranes. This ensures that the transport properties of In-M^{z+}/H^+ can be impacted only by the morphology and microstructure of the membranes. By changing the counter-cation, we tune the anion-cation interactions, inter-chains interactions, ionic block polarity and we expect to vary the compatibility between the two blocks, which are key factors determining the final morphology and microstructure of the membranes. We report the comprehensive analysis of these cation-dependent effects by combining proton conductivity, dynamic vapor sorption (DVS), dynamical mechanical analysis (DMA), small-angle neutron scattering (SANS) and field-emission electron microscopy (FE-SEM) characterizations, bringing insights on how to best optimize membrane transport properties by controlling the membrane microstructure/morphology through counter-cation selective manufacturing process.

2.1. Cation Influence on Membrane Morphology and Transport Properties

The alpha relaxation temperatures (T_α) measured by DMA give information on the polymer chain dynamics in the salt-form (In-M^{z+}) compounds (**Figure 2a-b**). The results show that T_α decreases linearly on increasing the size of alkali monovalent cations, which is in agreement with the results on Nafion reported by Bas et al.[40,41] Despite a very different cation size, the organic and proton counter-cation membranes, In-TEA^+ and In-H^+, exhibit close T_α values, lower than those of other monovalent cations, while the T_α of In-Ca^{2+} membranes is much higher, proving much stronger inter-chain interactions due to the divalent nature of calcium ion. The DMA results therefore clearly evidence that the nature of the cation has a direct impact on the strengths of inter-chain interactions as well as on the

phase separation. Note that In-Ca^{2+}, In-Cs^{+}, In-K^{+} and In-Li^{+} present a small peak around 220 °C corresponding to the relaxation of the hydrophobic phase, which is also observed in DMA curves of the acidified samples (**Figure S1**).[24,27]

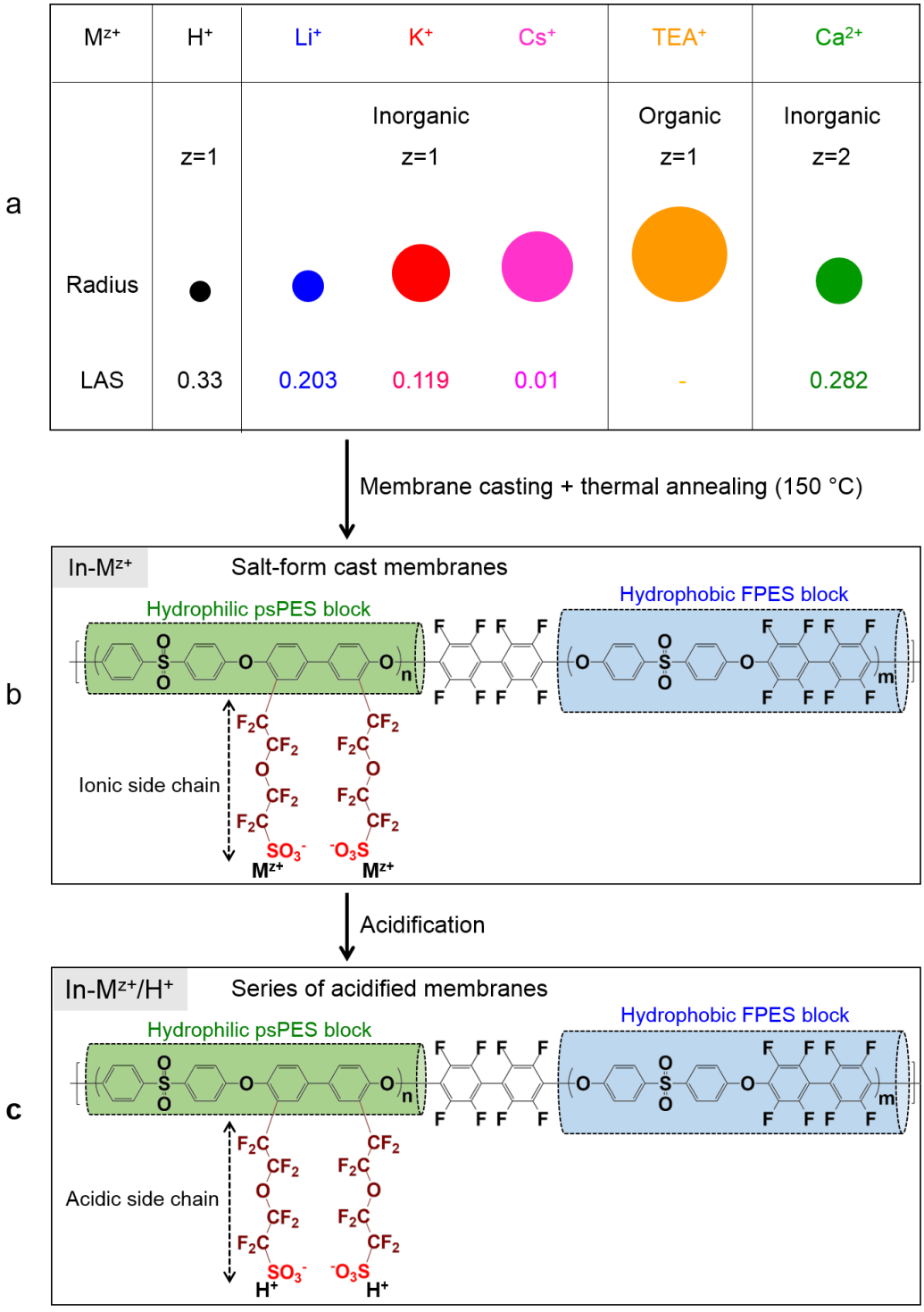

Figure 1. *(a) Cation selection for membrane manufacturing and their main properties, e.g. nature, valence, size and lewis acid strength (LAS): H^{+} (black), Li^{+} (blue), K^{+} (red), Cs^{+} (pink), TEA^{+} (orange) and Ca^{2+} (green). Chemical structure of In ionomer in salt form after casting, In-M^{z+} (b) and acidic form after acidification, In-M^{z+}/H^{+} (c). The ionomer is composed of a hydrophobic fluorinated*

polyether sulfone (FPES) block and hydrophilic psPES block carrying perfluorinated side-chains terminated by sulfonic acid group and counter cation.

The influence of counter-cation on acidified membrane water uptake and transport properties was further evaluated by measuring the vapor sorption and proton conductivity of acidified, In-M^{z+}/H^+, at 25 °C as a function of relative humidity (RH) (**Figure 2c–d**). The sorption isotherms of all In-M^{z+}/H^+ membranes, representing the number of water molecules per ionic group (labeled as λ) as a function of the relative humidity (RH), present similar shapes which are typical for these ionomers.[28] However, In-H^+/H^+ and In-TEA^+/H^+ show slightly lower hydration at high RH (**Figure 2c**), e.g., 7 water molecules per ionic group at 95% RH against 8-9 for all other compounds. In general, the proton conductivity of ionomer membranes strongly depends on the water uptake. Yet, the moderate reduction in hydration cannot explain the large variations of proton conductivity. Thus, conduction of the acidified membranes is found to vary significantly depending on the counter-cation selected for manufacturing. The membrane cast with Cs^+ cation shows the highest proton conductivity, while the membranes cast from TEA^+ and H^+ show the lowest proton conductivity. At 95% RH, for instance, In-Cs^+/H^+ is around 3.5 times more conductive than In-H^+/H^+ and In-TEA^+/H^+, an effect that is amplified at lower hydration (**Figure 2d**). Indeed, at low relative humidity (i.e., 10%) where the water uptake is similar for all compounds (λ~1.5-2), differences in conductivity by more than a factor 20 are found amongst the various cation-selective membranes.

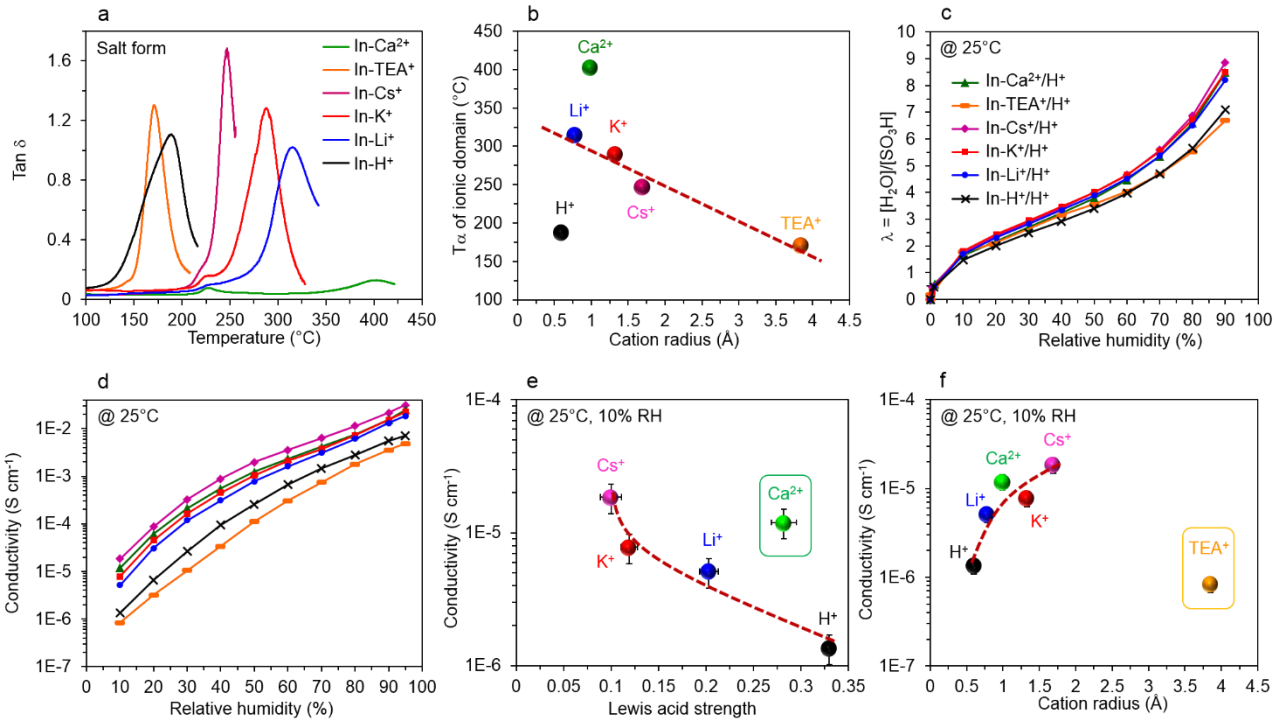

Figure 2. *a) DMA curves of salt-form In-M^{z+} ionomer bearing different counter cations. b) Relaxation temperature (T_α) of ionic domains of In-M^{z+} as a function of cation size. c) Sorption isotherms of*

acidified membranes expressed as the number of water molecules per ionic group (λ) as a function of relative humidity (DVS results) and d) proton conductivities of acidified membranes measured at 25 °C as a function of the relative humidity. Variations in proton conductivity of acidified membranes measured at 25 °C and 10% RH as a function of LAS (e) and cation radius (f). Dashed lines are guide to the eyes, allowing to evidence the anomalous behavior of Ca^{2+} and TEA^{+} compounds.

Interestingly, we observe that proton conductivity increases with the radius of cast monovalent inorganic cations, i.e., $H^+<Li^+<K^+<Cs^+$ and this trend was observed over the whole temperature range (**Figure S2**). Globally, the proton conductivity of the acidified membranes is strongly impacted by the nature of cation used for membrane casting. Danyliv et al.[42] reported a conductivity two time lower for a random copolymer cast with counter-cation K^+ than Li^+ but to our knowledge, there is any reported study on the impact of counter-cation on the proton conductivity of membranes based on block copolymers. **Figures 2e** and **Figure 2f** represent the proton conductivities measured at 25 °C at 10% RH, plotted in function of the cation LAS and radius, respectively. These representations are helpful to identify possible correlations between the cation characteristics and the functional property of the obtained acidified membranes. In fact, we observe that all cations seem to follow a general trend, i.e., the proton conductivity decreases with increasing LAS and increases with increasing cation radius, indicating the impact of both parameters on the realization of efficient conduction in the ionomers. However, there are two noticeable exceptions for In-Ca^{2+}/H^+ and In-TEA^+/H^+. Similar tendency was also observed for the conductivity measured at 60 °C, 95% RH, and at 25 °C, 60% RH as a function of LAS (**Figure S3a**) and cation radius (**Figure S3b**). These materials seem to have a peculiar behavior: i) despite the largest cation size, the conductivity of In-TEA^+/H^+ is much lower than that of In-Cs^+/H^+ sample, an effect that could be explained by the polarity and hydrophobicity of TEA^+, which may limit the formation and interconnection of conducting pathways, ii) by following the conductivity trend, it seems that, with equivalent cation size, the membrane cast with double-charge cation is more conductive than the one cast from mono-charge cation, which may relate to the stronger inter-chains interactions, as seen from the DMA results, and, consequently, a better organization of ionic domains. Hence, as both IEC and water uptake are comparable in all our membranes, it can be supposed that the huge differences in conductivity must result from cation-induced modifications of ionomer nanostructure and ionic domains tortuosity.

2.2. Morphology-Property Interplay

To evaluate this hypothesis, the morphologies of the acidified membranes were investigated by microscopy and scattering techniques, which both probe the typical sizes of phase-separated domains as well as the degree of long-range order in the materials. On **Figure 3** we represent the FESEM images

of dried membranes (**Figure 3a**), together with the corresponding SANS profiles (**Figure 3b**) of the same materials in dry (top) and hydrated (λ~20, bottom) states.

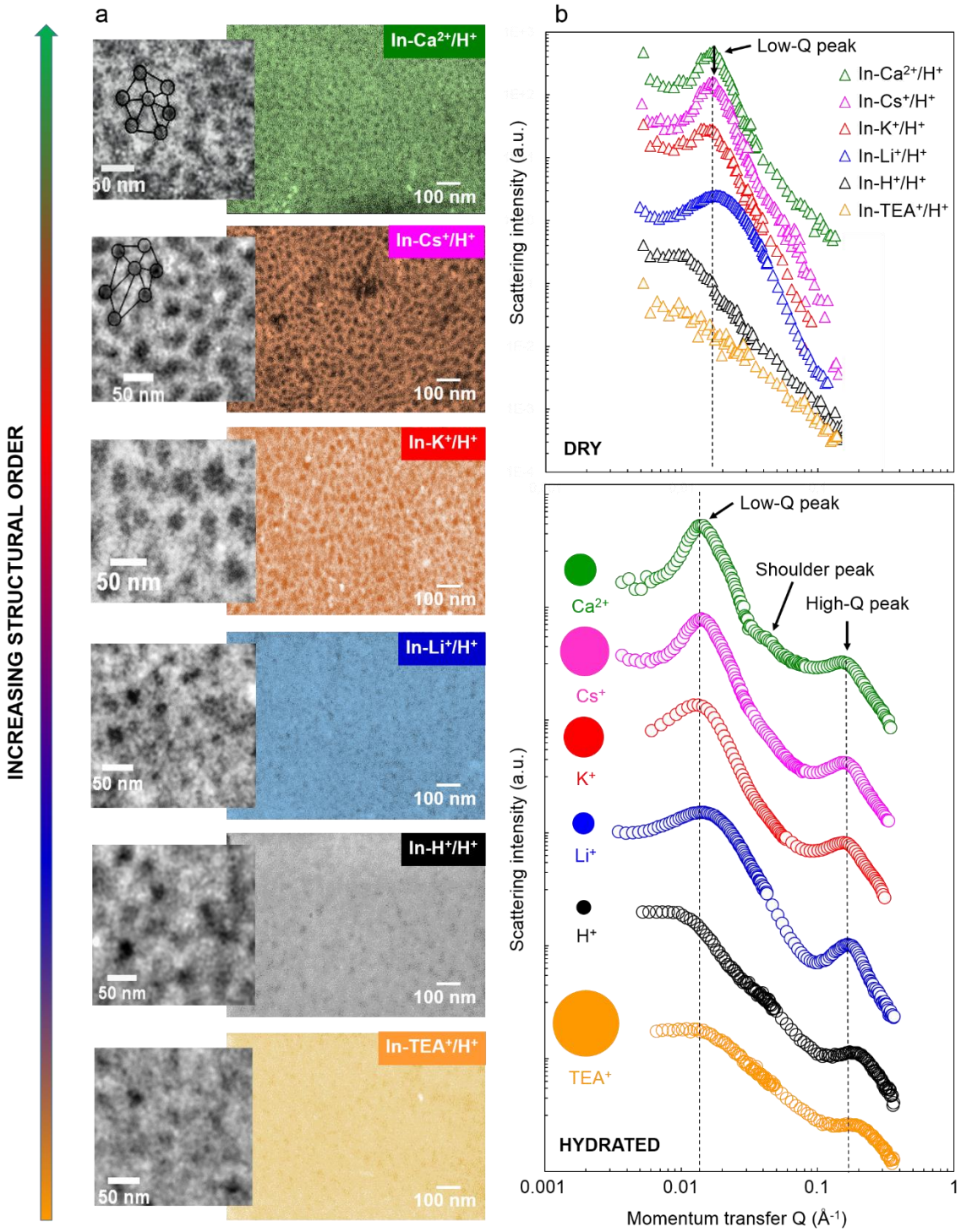

Figure 3. *a) FESEM micrographs of dried acidified ionomer films as a function of the cation used during manufacturing, presented from lowest (bottom, H^+ and TEA^+) to highest (top, Ca^{2+} and Cs^+) ordered structures. The insets show the segregation between hydrophobic (black) and hydrophilic (white) regions. In the case of Ca^{2+} and Cs^+, a local hexagonal arrangement is noticed. To enhance the contrast, protons of acidified membranes were exchanged by Pb^{2+} cations. b) Corresponding 1D*

SANS profiles in function of the scattering vector Q measured in dried (top) and hydrated (λ~20, bottom) membranes (the same cation-color code as FESEM images), showing the presence of low-Q peaks due to large-scale block structure and high-Q peaks due to the nanoscale organization of ionic domains. In case of Ca^{2+} and Cs^{+}, the additional shoulder peak may indicate regular packing of the blocks (hexagonal phase). The low-Q peak broadening on replacing Ca^{2+} by Cs^{+}, K^{+}, Li^{+}, H^{+}, TEA^{+} indicates enhanced disorder of the block superstructure, confirming the microscopy results.

The FESEM images reveal obvious differences on membrane microstructure as a function of counter-cation, as highlighted by ordering these data from best organized (top) to less organized (bottom) microstructures. The membrane cast from hydrophobic organic TEA^{+} cation shows the worst phase separation (orange). The other membranes cast from monovalent cations display a phase-separated microstructure with hydrophobic FPES domains (dark regions) dispersed into to a continuous hydrophilic psPES phase (white regions) (see **Figure 1b–c** for the chemical structure of FPES and psPES blocks). On increasing monovalent cation size ($H^{+}<Li^{+}<K^{+}<Cs^{+}$), the long-range ordering of phase-separated nanodomains improves. While In-H^{+}/H^{+} is poorly organized (grey), the hydrophobic domains adopt locally a hexagonal packing for the biggest cation Cs^{+} (brownish). The divalent Ca^{2+} cation leads to a similar microstructure to that of Cs^{+}, but with even more regular and better-defined hexagonal architecture (green). A statistical analysis of the FESEM images allowed to quantify both the mean diameter of PFES block domains (black nodules) and their polydispersity obtained from the full width at half maximum (FWHM) of the size distribution (**Figure S4a**). The nodule size follows a linear trend with cation size (**Figure S5**), except for In-H^{+}/H^{+} where the FPES size is bigger and the distribution much broader than for all other compounds.

These results are confirmed by the 1D SANS profiles *vs* scattering vector Q shown on **Figure 3b**, which contain the usual characteristic features of the block copolymers.[11,24] The low-Q correlation peak is due to long-range ordering between the hydrophilic psPES and hydrophobic FPES blocks, while the high-Q correlation peak (so-called ionomer peak) reflects the ionic domains organization, *i.e.*, nanoscale phase separation between the "ps" side chains and PES polymer main chains. Moreover, the high-Q intensity decay as Q^{-4} (so-called Porod's law) indicates the existence of sharp interfaces between the ionic network and PES chains. Note that the ionomer peak is revealed by the presence of water that swells the ionic domains and induces neutron contrast, while the block peak can be detected in both dry and hydrated states.[11] The peak positions Q_{block} and Q_{ionic} give the mean separation distance between block aggregates and ionic domains, d_{block} and d_{ionic} defined as $d=2\pi/Q_{block/ionic}$, respectively, while the relative widths $\Delta Q_{block}/Q_{block}$ and $\Delta Q_{iono}/Q_{iono}$ indicate the degree of order in the materials. The sharper the peak, the better organized is the material at the corresponding length scale, *i.e.*, typically > 35 nm for block superstructure and 2–5 nanometers for the ionic phase. On **Figure 3**, we

have classified the intensity-shifted 1D SANS scattering profiles following the FESEM increasing order. The visual inspection of the block peak shape confirms the decreasing large-scale order (increasing low-Q peak broadening) from Ca^{2+}, Cs^{+}, K^{+}, Li^{+}, H^{+} to TEA^{+}, in excellent agreement with the microscopy results. The In-TEA^{+}/H^{+} membrane has no block peak in dry state, and a broad, poorly defined one in hydrated state. The In-H^{+}/H^{+} compound is almost as disordered and, moreover, the block peak is shifted towards small Q values, reflecting the increased block separation distance compatible with the greatest size and broadest distribution of the hydrophobic nodules in this membrane (**Figure S5**). The best organization of block superstructure is found for the In-$Ca^{2+/}H^{+}$ and In-Cs^{+}/H^{+} membranes, for which the SANS data exhibit an additional shoulder peak (in medium-Q region ~0.039–0.042 $Å^{-1}$, corresponding to correlation distances of ~150–160 Å) compatible with an hexagonal arrangement as depicted in the corresponding FESEM images. These behaviors are better visualized on **Figure S4b-c** and **Figure S4d-e** where the block peak and ionomer peak regions are highlighted, respectively. The large-scale separation distance between hydrophobic blocks is similar in all membranes (**Figure S4b,** dashed line), except for In-H^{+}/H^{+}, as noticed before. The same data plotted using normalized $I/I_{peakmax}$ and $(Q-Q_{block})$ unit axis allow to observe directly the continuous increase in block peak width from Ca^{2+} to TEA^{+} (black arrow on **Figure S4c**). Similarly, we see that the ionic separation distances are almost unchanged, despite the utilization of cations with different sizes during membrane casting (**Figure S4d**, dashed line). Looking back to the literature on sulfonated polystyrene,[43,44] Nafion,[45–47] and random aromatic copolymers bearing perfluorosulfonic acid[42] we know that ion aggregation depends on the counter-cation size. Zhou et al.[43] found that the cation concentration in ionic aggregates with monovalent cations is 2–3 times higher than that of ionomers neutralized with divalent cations. Surprisingly, opposite behavior was reported for Nafion® N212 membrane, in which the SAXS intensity of both ionic peak and matrix-knee decreased with increasing cation size.[45] In those cases, however, the counter cations still remained inside the membrane, which is not the case here as our ionomers were completely acidified before characterization. Danyliv et al.[42] reported the hydrophilic domains in the acidified random copolymer membranes obtained from Li^{+} counter-cation are more homogeneous than those from K^{+}, for the last two types of the ionic clusters was evidence: one of a very high organization and the other of worse organization. In this work, we observe that the ionic peak widths are moderately affected by the nature of the casting counter cation (**Figure S4e**, black arrow), with In-TEA^{+}/H^{+} membrane still exhibiting the poorer nanoscale phase separation. Therefore, quite surprisingly, the choice of the cation has a limited impact on the local ionic structure.

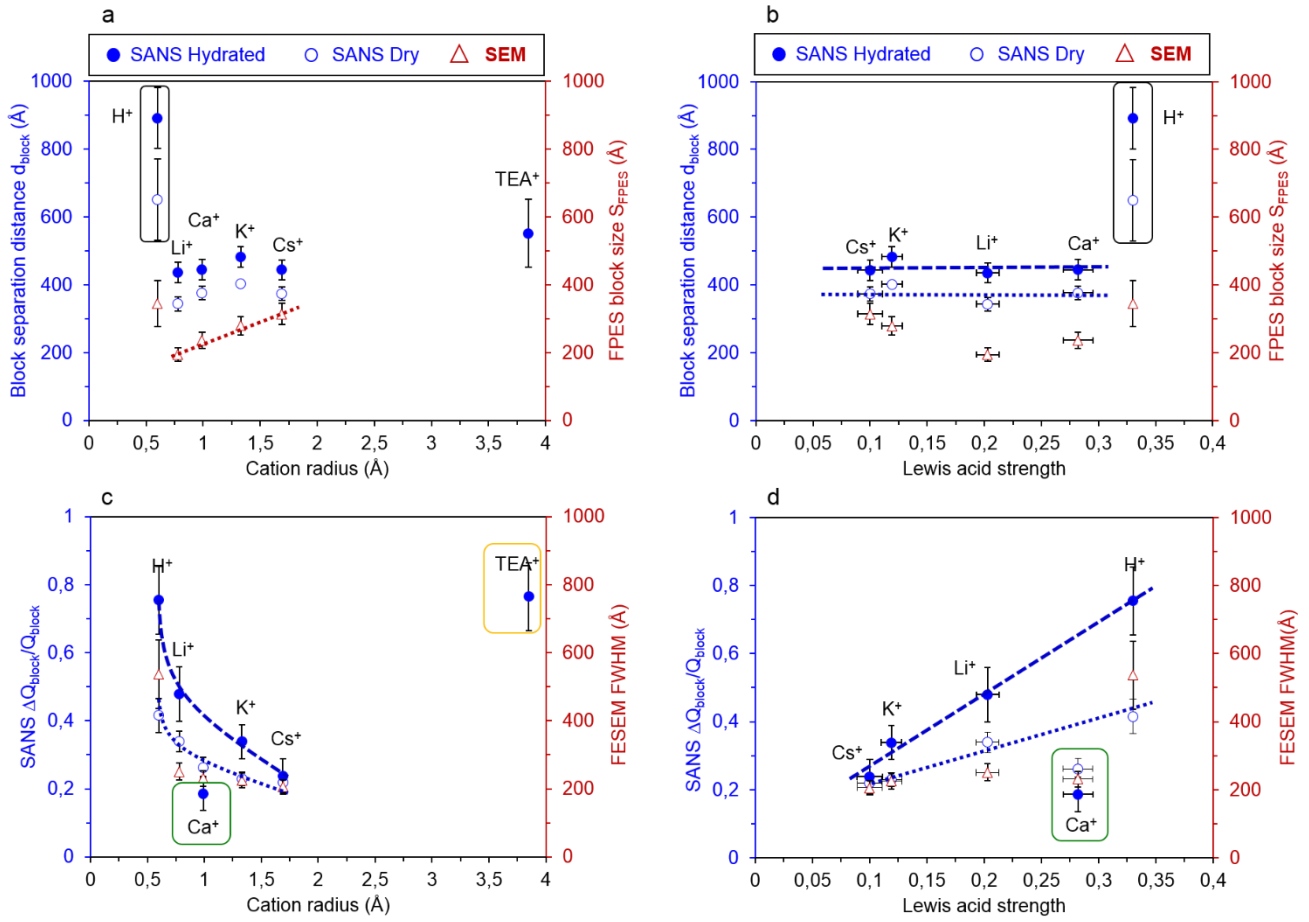

Figure 4. *Mean block separation distances (blue circles. Open symbols: dry and closed symbols: hydrated) and hydrophobic FPES cluster sizes (red triangles) determined from the Gaussian peak position of SANS data and SEM distribution, respectively, plotted in function of the cation radius (a) and LAS (b). FWHM of SANS ($\Delta Q_{block}/Q_{block}$) and SEM data in function of the cation radius (c) and LAS (d). Dashed lines are guide for the eyes, indicating the moderate variations in sizes/distances with cation features (a, b), and the master curve behaviors of order parameter (c, d). Noticeable anomalies are indicated by colored squares, e.g., H^+, TEA^+ and Ca^{2+} compounds deviate from the average behavior.*

By fitting the FESEM size distribution and SANS peaks with Gaussian functions (**Figure S6**), we can now examine the characteristic values extracted from microscopy and scattering techniques in more details. **Figure 4** displays the mean FPES cluster sizes S_{FPES} (SEM results, red triangles) and block separation distances d_{block} (SANS in dry and hydrated states, empty and full blue circles, respectively) in function of the cation radius (**Figure 4a**) and LAS (**Figure 4b**). First, we observe a strong correlation between the two experimental methods employed to quantify the evolution of phase separation as a function of counter-cation. The differences in absolute values obtained by SANS and FESEM in dry state are attributed to distinct definitions: mean diameter of hydrophobic block clusters in the case of FESEM (red triangles, ranging from 200 to 350 Å typically) and separation distance between two

scattering objects in SANS (blue circles). It seems that the superstructure spacing d_{block} is not much dependent on the nature of the casting counter-cation, except for H^+, a behavior that might not be ascribed to size effect only, as H^+ is very close to Li^+. The trend is that d_{block} and S_{FPES} slightly increase on increasing cation radius. Upon increasing hydration for all types of ionomers, values of d_{block} increase, as expected, up to around 400 Å at $\lambda = 20$, except for the In-TEA^+ (500 Å) and, particularly, for the H^+ ionomer which shows much larger distances (from 700 Å in dry state to 900 Å in hydrated state). By subtracting the cluster dimension from the separation distance, one can estimate the size of the ionic block regions (S_{ionic} defined as $d_{block}–S_{FPES}$**, Figure S5**, green squares). Values are found in the range of ~130 Å for dried membranes and ~200 Å for hydrated ionomers. Again, the anomalous behavior of In-H^+/H^+ is clear. Note also that Cs^+, which is the largest and most hydrophobic alkaline cation, yields the smallest ionic block domains size. Regarding the degree of order in the materials, the evolution of FWHM of FESEM distributions and relative FWHM of scattering peaks in function of LAS and cation radius nicely correlate (**Figure 4c-d**). The behavior of all cations follows a trend (symbolized by dashed lines), except for Ca^{2+} and TEA^+. Interestingly, In-H^+/H^+ sample does not deviate from the general trend regarding the level of organization. On increasing the cation radius, there is a clear diminution of the FWHM, indicating that a more homogenous and better-defined nano-structuration is formed when bigger cations were used during membrane casting. On increasing LAS, in contrast, we see an almost linear increase of FWHM values, showing that higher polarizability is not favorable to obtain ordered block morphologies. The deviation of In-Ca^{2+}/H^+ and In-TEA^+/H^+ from the main trend is quite insightful, as it shows that there is a direct impact of both size (TEA^+ is so big that it is out of the main curve) and bonding (divalent is out of the trend). Moreover, the TEA^+ cation is organic in nature and hydrophobic. Since our ionomers were completely acidified before characterization, the changes in FWHM from SANS and SEM measurements is exclusively linked to the membrane microstructure.

To summarize, we have fully characterized the multiscale structure of the In-M^{z+}/H^+ membranes and we can conclude that there is a relatively limited impact of cation selection on the nanoscale organization of ionic domains within the ionic blocks, while it has a strong influence on the structural arrangements at larger scale where polymer blocks segregate. Therefore, it can be supposed that the counter-cation plays an important role on the thermodynamic interactions between the copolymer and solvent, and between the two copolymer blocks. These observations allow to assess the prominent role of the counter cation in the self-assembly process by acting as an effective facilitator agent (Ca^{2+}, Cs^+), a fair facilitator agent (K^+, Li^+) or a preventer agent (H^+, TEA^+), yielding either high-quality or poor-quality phase-separated morphologies. Cations therefore can help in separating the two blocks of the polymers or, on the contrary, attenuate their by-design incompatibility. These facilitating or preventing

abilities towards forming highly ordered block superstructures may arise from different properties. TEA^+ is the largest counter cation, but also the more hydrophobic, organic in nature, therefore it can act as a compatibilizer between the hydrophilic and hydrophobic blocks, leading to poor separation. Note that TEA^+ hydrophobicity also slightly degrades the local organization of ionic functions separated from the polymer main chains to form the ionic clusters. Regarding membrane cast from H^+, the poor phase separation and bigger block size could arise from the formation of a partially crosslinked structure during thermal annealing at 150 °C, due to the dehydration between two intermolecular perfluorosulfonic groups.[27] This behavior can be evidenced from DMA curves of all acidified membranes by an increase of storage modulus above 165 °C (**Figure S1**). However, the amount of acidic function lost after thermal annealing is very small as this sample has similar IEC than the others and was completely soluble in DMAc. Regarding Ca^{2+}, we observed that the In-Ca^{2+}/H^+ membrane exhibits a lower block size and a more homogenous distribution than its K^+ analogue, although K^+ is in the same row as Ca^{2+} in the periodic table and has a bigger size. Hence, we may hypothesize that the divalent nature of the ion is a key property towards block segregation and, consequently, induces the excellent behavior of In-Ca^{2+}/H^+ membrane.

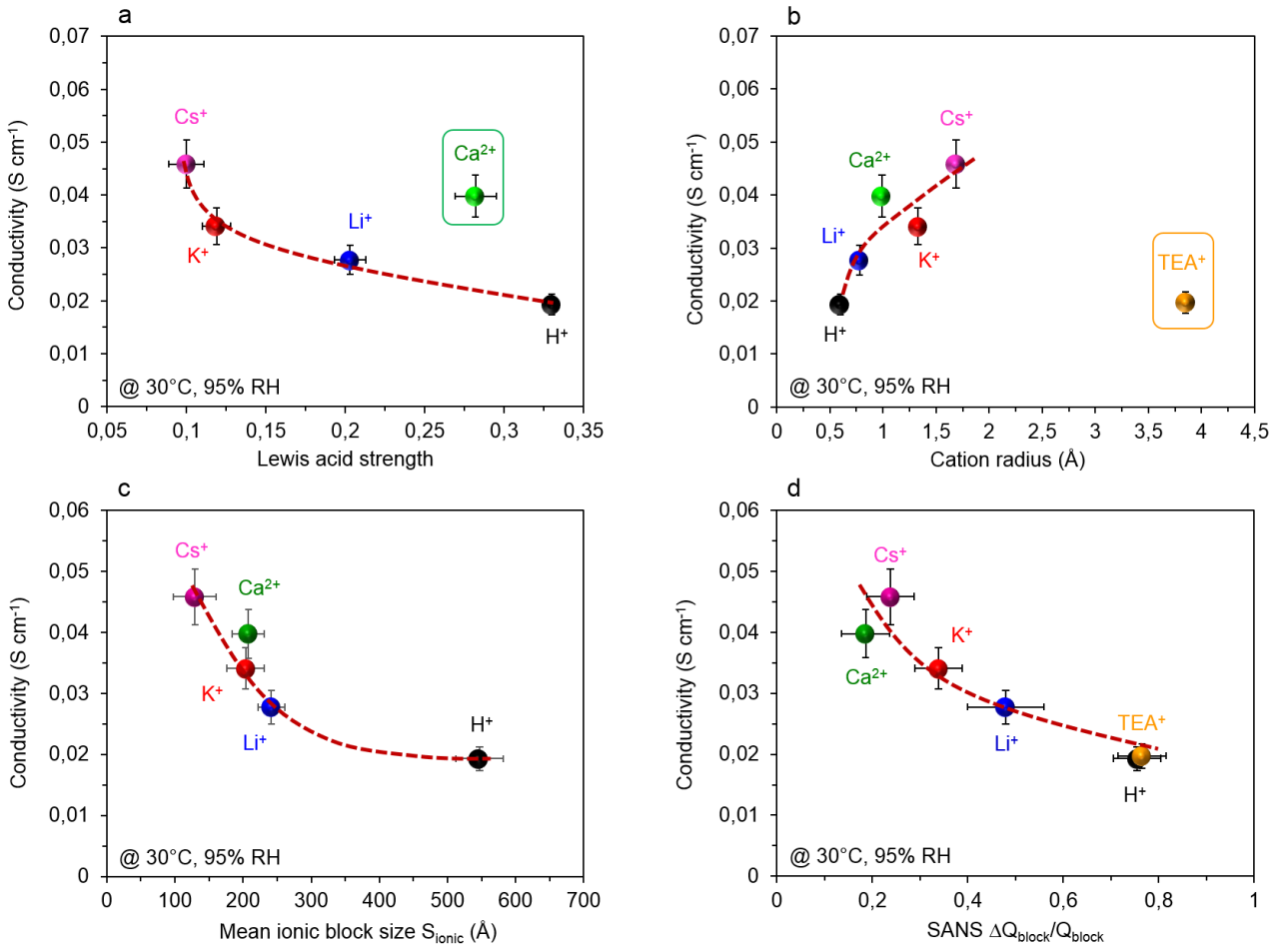

Figure 5. *Proton conductivity at 30 °C and 95% RH of the various acidified ionomers as a function of the LAS (a) and the cation radius (b), showing the anomalous behavior of Ca^{2+} and TEA^+-cast*

membranes. Same data as a function of structural parameters, e.g. the mean ionic block size S_{ionic} (c) and the order parameter $\Delta Q_{block}/Q_{block}$ (d). Dashed lines are guide to the eyes, showing the master curve behavior followed by all cation-types cast membranes when using the structural features as key monitoring parameters for transport efficiency

Considering the in-depth structural characterization, we can revisit our understanding of the functional behavior of the polymers, e.g., their efficiency as proton conductors. On **Figure 5a-b**, we show the variations of proton conductivity at 30 °C and 95% RH as a function of the cation LAS (**Figure 5a**) and radius (**Figure 5b**), *e.g.*, the usual representation we already adopted in **Figure 2e-f** (at 25 °C, 10% RH) and **Figure S3** (at 60 °C, 95% RH, and at 25 °C, 60% RH), and we compare it to a direct structure-transport correlative representation produced by plotting the same conductivity data in function of relevant structural parameters (**Figure 5c-d**). As such, we select the mean ionic block domain size, S_{ionic} (**Figure 5c**), which quantifies the mean extension of the connected phase where protons are transported, and the order parameter $\Delta Q_{block}/Q_{block}$ (**Figure 5d**) that characterizes the quality of hydrophobic block/hydrophilic block phase separation. We see that the conductivity continuously increases with decreasing ionic domain size and increasing long-range structural order (or decreasing FWHM).

Although Ca^{2+} and TEA^{+} based materials have a peculiar behavior when considering cation characteristics as the monitoring parameter (**Figure 5a-b**), this is not any more the case when we rather consider structural parameters as key factors influencing proton transport. In fact, both anomalous compounds now fall on the general curve materialized by the dashed lines in **Figures 5c-d**. It seems that the conductivity of In-Ca^{2+}/H^{+} also follows the monovalent-cation trend. The structure-property interplay confirms the assumption about better defined and more regular ionic blocks domains via using larger cation sizes, which results in more homogeneous ps-PES domains with enhanced long-range connectivity, which is critical to improve the proton transport through the membrane. As discussed earlier, the lower the hydration level of the membrane, the higher the conductivity gap among the samples. Therefore, greatest differences in membrane proton conductivity were observed at reduced RH (**Figure 2e-f**). If we analyze the 10%-RH conductivity results using the dried membranes structural parameters, we obtain similar trends (**Figure S7**), showing the robustness of the conclusions.

3. Conclusions

In summary, the counter-cation used during membrane manufacturing has a strong impact on both the morphology and the functional properties of acidified aromatic ionomer membranes. The cation influence is more pronounced on the large-scale phase separation between the hydrophilic and

hydrophobic blocks (~40 nm) than on the small-scale phase separation between the ionic side chain and the polymer main chain (~3–5 nm) where they have direct interaction. Indeed, the characteristics of the counter cations, i.e., their size, charge, organic vs inorganic nature, hydrophobicity and Lewis acid strength, play a key role in the self-assembly process by tuning the constitutive copolymer blocks incompatibility, therefore aiding or preventing efficient block segregation. The organization of the block superstructure improves on increasing the size and the charge of counter cations, while it degrades with increasing Lewis acid strength. Interestingly, the membranes cast with the smallest (H^+) and largest (TEA^+) counter cation have similar morphology and proton-transport properties. Both have quite disordered nanostructures due to the poor phase separation between the hydrophilic and hydrophobic blocks which results in much lower proton conductivity than the materials cast with alkaline counter cations. The acidified membrane cast with Cs^+ cation shows the highest proton conductivity due to the high-quality phase separated block superstructure formed by the regular packing of well-defined hydrophobic objects. The divalent Ca^{2+} cation is also acting as an efficient structuring agent yielding excellent functional performances to the ionomer. With this work, we showed a simple-but-effective method to control the morphology and functional properties of aromatic ionomers for advanced applications.

4. Experimental

4.1. Membrane Preparation

The mixture of 1.0 g ionomer powder in 14 ml of DMAc was (i) stirred at 60 °C for 24 h, (ii) left under vacuum for eliminating gas bubbles, (iii) centrifuged at 5000 rpm for removing solid impurities to obtain homogeneous solution. The solution was cast onto a glass substrate using an Elcometer 4340 Automatic Film Applicator. The “as-cast” membranes, obtained after drying at 60 °C in an oven for 24 h, were submitted to a thermal annealing by following a procedure described elsewhere.[24,32] The obtained membranes was immersed in distilled water for 24 h to remove solvent residue and acidified two times using 2 M aqueous HCl solution, followed by washing several times with distilled water to remove acid trace. The In-H^+ membrane cast directly from ionomer in acidic form was also realized with the same condition for comparison.

4.2. Characterization

The IEC was measured by acid-base titration in organic medium as described elsewhere.[48] The DMA was performed on Q800 system (TA Instruments) with a heating rate of 2 °C/min in temperature range (i) from 30 to 270 °C for acidified membranes, and (ii) from 30 to 150–400 °C for salt-form membranes depending of the Tg of the ps-PES hydrophilic block. The DVS was determined at 25 °C from 0 to 90% by steps of 10% using a DVS IGASORP (Hiden Isochema, UK). The samples (~50 mg) were

previously dried in the instrument by exposing to 0% RH at 80 °C for 8 h. The FESEM was analyzed with a back scattered detector (very sensitive to atomic number of atoms present in the material) by a ZEISS Ultra 55 device on dried lead-salt membranes. To increase the contrast between hydrophilic and hydrophobic domains, the proton in acidified membranes was exchanged by Pb^{2+} cation. The dark regions correspond to hydrophobic domains whereas the hydrophilic domains are clear on these images. ImageJ "open source" software was used for the image analysis: a tailored procedure, which iterates a binarization, a watershed segmentation and a particle analysis, furnished the size distributions of FPES blocks. For one sample, three images with two magnifications were post-treated to further increase the image contrast and analyze the size distribution of the hydrophobic and hydrophilic domains. The SANS analysis was performed on D22 spectrometer (Institut Laue-Langevin, Grenoble, France) and on PAXY spectrometer (Laboratoire Léon-Brillouin, Paris, France). All measurements were conducted on fully-hydrated acidified membranes using experimental set-up and data reduction as described elsewhere.[24,27] The through-plane proton conductivity (σ) were obtained from a lab-made conductivity cell[11] using a Material Mates 7260 analyzer from 5 Hz to 10 MHz. The acidified ionomer films (≈60–80 μm in thickness) were sandwiched between two stainless steel electrodes (blocking electrodes). The conductivity measurements were carried out (i) at 25 °C as a function of RH from 10 to 90% with step of 10% and (ii) at 95% as a function of cell temperature from 30 to 90 °C with step of 10 °C. The samples were stabilized at measuring condition for 5 h prior to measurement and Zview software was used to analyze and fit the data. The equivalent circuit and fitting parameters were depicted elsewhere.[11] The conductivity was calculated by **Equation 1**:

$$\sigma = \frac{L}{R \times S} \qquad (\mathbf{1})$$

where L is sample thickness, S is upper electrode surface area, and R is bulk membrane resistance.

ASSOCIATED CONTENT

Supporting Information. *Cation radius, Lewis acid strength, and IEC of acidified membranes. Storage modulus and tan δ of acidified ionomer films. Proton conductivity measured at 95% RH as a function of temperature. Proton conductivity as a function of LAS and cation radius measured at 60 °C, 95% RH and at 25 °C, 60% RH. Structural characteristics of In-M^+/H^+ membranes. Variations of the ionic block domains size as a function of cation radius and Lewis acid strength. Low-Q peak fitting of SANS data with a Gaussian peak and a background. Proton conductivity measured at 25 °C, 10% RH as a function of mean ionic block size obtained using the relation $S_{ionic}=d_{block}-S_{FPES}$.* This material is available free of charge via the internet at http://pubs.acs.org.

AUTHOR INFORMATION

Corresponding Author

C. Iojoiu (Cristina.Iojoiu@lepmi.grenoble-inp.fr)

S. Lyonnard (sandrine.lyonnard@cea.fr)

Author Contributions

C.I. designed the concept. H.-D.N. synthesized the polymer, prepared the samples, and performed the NMR, SEC, DSC, DMA, and proton-conductivity measurements. C.I., S.L., H.-D.N., and T.K.L.N. carried out the SANS measurements and treated the data. E.P. performed the DVS measurements. T.K.L.N. performed the FESEM measurements. C.I. and S.L. supervised the project. H.-D.N., C.I. and S.L. wrote the manuscript. All authors revised the final version of the manuscript.

Notes

The authors declare no competing financial interest.

ACKNOWLEDGMENT

The authors acknowledge the Institut Laue-Langevin (ILL, Grenoble, France) and Laboratoire Léon Brillouin (LLB, CEA Saclay, France) for providing the neutron facilities used in this work via proposal numbers 9-11-1709 (DOI: doi:10.5291/ILL-DATA.9-11-1709) and 150, respectively. The authors acknowledge the financial support from the French National Research Agency within the NSPEM project (ANR-16-CE05-0016), and the Centre of Excellence of Multifunctional Architectured Materials “CEMAM” AN-10-LABX-44−01).

REFERENCES

(1) Ghassemi, H.; McGrath, J. E.; Zawodzinski, T. A. Multiblock Sulfonated–Fluorinated Poly(Arylene Ether)s for a Proton Exchange Membrane Fuel Cell. *Polymer (Guildf).* **2006**, *47*, 4132–4139.

(2) Yu, X.; Roy, A.; Dunn, S.; Badami, A. S.; Yang, J.; Good, A. S.; Mcgrath, J. E. Synthesis and Characterization of Sulfonated-Fluorinated, Hydrophilic-Hydrophobic Multiblock Copolymers for Proton Exchange Membranes. *J. Polym. Sci. Part A Polym. Chem.* **2009**, *47*, 1038–1051.

(3) Li, N.; Lee, S. Y.; Liu, Y.-L.; Lee, Y. M.; Guiver, M. D. A New Class of Highly-Conducting Polymer Electrolyte Membranes: Aromatic ABA Triblock Copolymers. *Energy Environ. Sci.* **2012**, *5* (1), 5346–5355.

(4) Weiber, E. A.; Meis, D.; Jannasch, P. Anion Conducting Multiblock Poly(Arylene Ether Sulfone)s Containing Hydrophilic Segments Densely Functionalized with Quaternary Ammonium Groups. *Polym. Chem.* **2015**, *6*, 1986–1996.

(5) Liu, L.; Huang, G.; Kohl, P. A. Anion Conducting Multiblock Copolymers with Multiple Head-Groups. *J. Mater. Chem. A* **2018**, *6* (19), 9000–9008.

(6) Li, Q.; Chen, Y.; Rowlett, J. R.; McGrath, J. E.; Mack, N. H.; Kim, Y. S. Controlled Disulfonated Poly(Arylene Ether Sulfone) Multiblock Copolymers for Direct Methanol Fuel Cells. *ACS Appl. Mater. Interfaces* **2014**, *6* (8), 5779–5788.

(7) Xue, B.; Zhou, S.; Yao, J.; Wang, F.; Zheng, J.; Li, S.; Zhang, S. Novel Proton Exchange Membranes Based on Sulfonated-Phosphonated Poly (p-Phenylene-Co-Aryl Ether Ketone) Terpolymers with Microblock Structures for Passive Direct Methanol Fuel Cells. *J. Memb. Sci.* **2020**, *594*, 117466.

(8) Hong, S. H.; Cha, M. S.; Hong, S.-K.; Oh, S.-G.; Lee, J. Y. Structural Effect of the Hydrophobic Block on the Chemical Stability of Ion-Conducting Multiblock Copolymers for Flow Battery. *ACS Sustain. Chem. Eng.* **2019**, *7* (20), 17088–17099.

(9) Porcarelli, L.; Shaplov, A. S.; Salsamendi, M.; Nair, J. R.; Vygodskii, Y. S.; Mecerreyes, D.; Gerbaldi, C. Single-Ion Block Copoly(Ionic Liquid)S As Electrolytes for All-Solid State Lithium Batteries. *ACS Appl. Mater. Interfaces* **2016**, *8*, 10350–10359.

(10) Nguyen, H.-D.; Kim, G.-T.; Shi, J.; Paillard, E.; Judeinstein, P.; Lyonnard, S.; Bresser, D.; Iojoiu, C. Nanostructured Multi-Block Copolymer Single-Ion Conductors for Safer High-Performance Lithium Batteries. *Energy Environ. Sci.* **2018**, *11* (11), 3298–3309.

(11) Nguyen, H. D.; Assumma, L.; Judeinstein, P.; Mercier, R.; Porcar, L.; Jestin, J.; Iojoiu, C.;

Lyonnard, S. Controlling Microstructure-Transport Interplay in Highly Phase-Separated Perfluorosulfonated Aromatic Multiblock Ionomers via Molecular Architecture Design. *ACS Appl. Mater. Interfaces* **2017**, *9* (2), 1671–1683.

(12) Li, N.; Wang, C.; Lee, S. Y.; Park, C. H.; Lee, Y. M.; Guiver, M. D. Enhancement of Proton Transport by Nanochannels in Comb-Shaped Copoly(Arylene Ether Sulfone)S. *Angew. Chemie* **2011**, *123* (39), 9324–9327.

(13) Shin, D. W.; Guiver, M. D.; Lee, Y. M. Hydrocarbon-Based Polymer Electrolyte Membranes: Importance of Morphology on Ion Transport and Membrane Stability. *Chem. Rev.* **2017**, *117*, 4759–4805.

(14) Li, N.; Guiver, M. D. Ion Transport by Nanochannels in Ion-Containing Aromatic Copolymers. *Macromolecules* **2014**, *47* (7), 2175–2198.

(15) Peckham, T. J.; Holdcroft, S. Structure-Morphology-Property Relationships of Non-Perfluorinated Proton-Conducting Membranes. *Adv. Mater.* **2010**, *22*, 4667–4690.

(16) He, G.; Li, Z.; Zhao, J.; Wang, S.; Wu, H.; Guiver, M. D.; Jiang, Z. Nanostructured Ion-Exchange Membranes for Fuel Cells: Recent Advances and Perspectives. *Adv. Mater.* **2015**, *27* (36), 5280–5295.

(17) Bates, F. S.; Fredrickson, G. H. Block Copolymer Thermodynamics: Theory And Experiment. *Annu. Rev. Phys. Chem.* **1990**, *41* (1), 525–557.

(18) Mai, Y.; Eisenberg, A. Self-Assembly of Block Copolymers. *Chem. Soc. Rev.* **2012**, *41* (18), 5969–5985.

(19) Park, C. H.; Lee, C. H.; Guiver, M. D.; Lee, Y. M. Sulfonated Hydrocarbon Membranes for Medium-Temperature and Low-Humidity Proton Exchange Membrane Fuel Cells (PEMFCs). *Prog. Polym. Sci.* **2011**, *36* (11), 1443–1498.

(20) Zhang, H.; Shen, P. K. Recent Development of Polymer Electrolyte Membranes for Fuel Cells. *Chem. Rev.* **2012**, *112*, 2780–2832.

(21) Varcoe, J. R.; Atanassov, P.; Dekel, D. R.; Herring, A. M.; Hickner, M. A.; Kohl, P. A.; Kucernak, A. R.; Mustain, W. E.; Nijmeijer, K.; Scott, K.; Xu, T.; Zhuang, L. Anion-Exchange Membranes in Electrochemical Energy Systems. *Energy Environ. Sci.* **2014**, *7*, 3135–3191.

(22) Li, X.; Zhang, H. H.; Mai, Z.; Zhang, H. H.; Vankelecom, I. Ion Exchange Membranes for Vanadium Redox Flow Battery (VRB) Applications. *Energy Environ. Sci.* **2011**, *4* (4), 1147.

(23) Lee, M.; Park, J. K.; Lee, H. S.; Lane, O.; Moore, R. B.; McGrath, J. E.; Baird, D. G. Effects of

Block Length and Solution-Casting Conditions on the Final Morphology and Properties of Disulfonated Poly(Arylene Ether Sulfone) Multiblock Copolymer Films for Proton Exchange Membranes. *Polymer (Guildf).* **2009**, *50* (25), 6129–6138.

(24) Assumma, L.; Nguyen, H. D.; Iojoiu, C.; Lyonnard, S.; Mercier, R.; Espuche, E. Effects of Block Length and Membrane Processing Conditions on the Morphology and Properties of Perfluorosulfonated Poly(Arylene Ether Sulfone) Multiblock Copolymer Membranes for PEMFC. *ACS Appl. Mater. Interfaces* **2015**, *7* (25), 13808–13820.

(25) Fan, Y.; Cornelius, C. J.; Lee, H.-S.; McGrath, J. E.; Zhang, M.; Moore, R.; Staiger, C. L. The Effect of Block Length upon Structure, Physical Properties, and Transport within a Series of Sulfonated Poly(Arylene Ether Sulfone)S. *J. Memb. Sci.* **2013**, *430*, 106–112.

(26) Mikami, T.; Miyatake, K.; Watanabe, M. Synthesis and Properties of Multiblock Copoly(Arylene Ether)s Containing Superacid Groups for Fuel Cell Membranes. *J. Polym. Sci. Part A Polym. Chem.* **2011**, *49* (2), 452–464.

(27) Assumma, L.; Iojoiu, C.; Mercier, R.; Lyonnard, S.; Nguyen, H. D.; Planes, E. Synthesis of Partially Fluorinated Poly(Arylene Ether Sulfone) Multiblock Copolymers Bearing Perfluorosulfonic Functions. *J. Polym. Sci. Part A Polym. Chem.* **2015**, *53* (16), 1941–1956.

(28) Nguyen, H. D.; Porihel, R.; Brubach, J. B.; Planes, E.; Soudant, P.; Judeinstein, P.; Porcar, L.; Lyonnard, S.; Iojoiu, C. Perfluorosulfonyl Imide versus Perfluorosulfonic Acid Ionomers in Proton-Exchange Membrane Fuel Cells at Low Relative Humidity. *ChemSusChem* **2020**, *13*, 590–600.

(29) Lee, H.-F.; Killer, M.; Britton, B.; Wu, Y.; Nguyen, H.-D.; Iojoiu, C.; Holdcroft, S. Fuel Cell Catalyst Layers and Membrane-Electrode Assemblies Containing Multiblock Poly(Arylene Ether Sulfones) Bearing Perfluorosulfonic Acid Side Chains. *J. Electrochem. Soc.* **2018**, *165* (10), F891–F897.

(30) Kreuer, K. D. On the Development of Proton Conducting Polymer Membranes for Hydrogen and Methanol Fuel Cells. *J. Memb. Sci.* **2001**, *185* (1), 29–39.

(31) Lee, C. H.; Lee, K.-S.; Lane, O.; McGrath, J. E.; Chen, Y.; Wi, S.; Lee, S. Y.; Lee, Y. M. Solvent-Assisted Thermal Annealing of Disulfonated Poly(Arylene Ether Sulfone) Random Copolymers for Low Humidity Polymer Electrolyte Membrane Fuel Cells. *RSC Adv.* **2012**, *2* (3), 1025–1032.

(32) Nguyen, H.-D.; Jestin, J.; Porcar, L.; Iojoiu, C.; Lyonnard, S. Aromatic Copolymer/Nafion Blends Outperforming the Corresponding Pristine Ionomers. *ACS Appl. Energy Mater.* **2018**, *1*

(2), 355–367.

(33) Lee, K. H.; Cho, D. H.; Kim, Y. M.; Moon, S. J.; Seong, J. G.; Shin, D. W.; Sohn, J. Y.; Kim, J. F.; Lee, Y. M. Highly Conductive and Durable Poly(Arylene Ether Sulfone) Anion Exchange Membrane with End-Group Cross-Linking. *Energy Environ. Sci.* **2017**, *10* (1), 275–285.

(34) Kim, K.; Heo, P.; Hwang, W.; Baik, J.-H.; Sung, Y.-E.; Lee, J.-C. Cross-Linked Sulfonated Poly(Arylene Ether Sulfone) Containing a Flexible and Hydrophobic Bishydroxy Perfluoropolyether Cross-Linker for High-Performance Proton Exchange Membrane. *ACS Appl. Mater. Interfaces* **2018**, *10* (26), 21788–21793.

(35) Kim, K.; Heo, P.; Han, J.; Kim, J.; Lee, J.-C. End-Group Cross-Linked Sulfonated Poly(Arylene Ether Sulfone) via Thiol-Ene Click Reaction for High-Performance Proton Exchange Membrane. *J. Power Sources* **2018**, *401*, 20–28.

(36) Kallitsis, K. J.; Nannou, R.; Andreopoulou, A. K.; Daletou, M. K.; Papaioannou, D.; Neophytides, S. G.; Kallitsis, J. K. Crosslinked Wholly Aromatic Polyether Membranes Based on Quinoline Derivatives and Their Application in High Temperature Polymer Electrolyte Membrane Fuel Cells. *J. Power Sources* **2018**, *379*, 144–154.

(37) Liu, D.; Yates, M. Z. Tailoring the Structure of S-PEEK/PDMS Proton Conductive Membranes through Applied Electric Fields. *J. Memb. Sci.* **2008**, *322* (1), 256–264.

(38) Zhao, S.; Ren, J.; Wang, Y.; Zhang, J. Electric Field Processing to Control the Structure of Titanium Oxide/Sulfonated Poly (Ether Ether Ketone) Hybrid Proton Exchange Membranes. *J. Memb. Sci.* **2013**, *437*, 65–71.

(39) Wang, D.; Chen, N.; Long, C.; Lu, C.; Li, Y.; Zhu, H.; Wang, F. Electric-Field-Aligned Functionalized-Layered Double Hydroxide/Polyphenyl Ether Composite Membrane for Ion Transport. *Int. J. Hydrogen Energy* **2019**, *44* (26), 13852–13863.

(40) Moukheiber, E.; Bas, C.; Alberola, N. D.; Flandin, L. Infrared and Thermal Behaviour of Proton Exchange Membrane (PEM) after Cationic Contamination. *J. Memb. Sci.* **2013**, *431*, 105–112.

(41) Bas, C.; Reymond, L.; Danérol, A.-S.; Albérola, N.; Rossinot, E.; Flandin, L. Key Counter Ion Parameters Governing Polluted Nafion Membrane Properties. *J. Polym. Sci. Part B Polym. Phys.* **2009**, *47*, 1381–1392.

(42) Danyliv, O.; Iojoiu, C.; Lyonnard, S.; Sergent, N.; Planes, E.; Sanchez, J.-Y. Highly Phase Separated Aromatic Ionomers Bearing Perfluorosulfonic Acids by Bottom-up Synthesis: Effect of Cation on Membrane Morphology and Functional Properties. *Macromolecules* **2016**, *49* (11), 4164–4177.

(43) Zhou, N. C.; Chan, C. D.; Winey, K. I. Reconciling STEM and X-Ray Scattering Data to Determine the Nanoscale Ionic Aggregate Morphology in Sulfonated Polystyrene Ionomers. *Macromolecules* **2008**, *41* (16), 6134–6140.

(44) Jeon, H. S.; Kim, J. S. Dynamic Mechanical Properties and Morphology of Sulfonated Polystyrene Ionomers Neutralized with Mixtures of Various Cations. *Polym. Bull.* **2003**, *49* (6), 457–464.

(45) Shi, S.; Weber, A. Z.; Kusoglu, A. Structure-Transport Relationship of Perfluorosulfonic-Acid Membranes in Different Cationic Forms. *Electrochim. Acta* **2016**, *220*, 517–528.

(46) Peng, J.; Tian, M.; Cantillo, N. M.; Zawodzinski, T. The Ion and Water Transport Properties of K+ and Na+ Form Perfluorosulfonic Acid Polymer. *Electrochim. Acta* **2018**, *282*, 544–554.

(47) Peng, J.; Lou, K.; Goenaga, G.; Zawodzinski, T. Transport Properties of Perfluorosulfonate Membranes Ion Exchanged with Cations. *ACS Appl. Mater. Interfaces* **2018**, *10* (44), 38418–38430.

(48) Iojoiu, C.; Genova-Dimitrova, P.; Maréchal, M.; Sanchez, J.-Y. Chemical and Physicochemical Characterizations of Ionomers. *Electrochim. Acta* **2006**, *51* (23), 4789–4801.

TOC Graphic